

Provided for non-commercial research and education use.
Not for reproduction, distribution or commercial use.



This article appeared in a journal published by Elsevier. The attached copy is furnished to the author for internal non-commercial research and education use, including for instruction at the authors institution and sharing with colleagues.

Other uses, including reproduction and distribution, or selling or licensing copies, or posting to personal, institutional or third party websites are prohibited.

In most cases authors are permitted to post their version of the article (e.g. in Word or Tex form) to their personal website or institutional repository. Authors requiring further information regarding Elsevier's archiving and manuscript policies are encouraged to visit:

<http://www.elsevier.com/copyright>



Contents lists available at ScienceDirect

Computational Materials Science

journal homepage: www.elsevier.com/locate/commsatsci

Determination of the phase diagram from interatomic potentials: The iron–chromium case

G. Bonny^{a,*}, R.C. Pasianot^{b,c,d}, E.E. Zhurkin^e, M. Hou^f

^a SCK•CEN, Nuclear Materials Science Institute, Boeretang 200, B-2400 Mol, Belgium

^b CAC-CNEA, Depto. de Materiales, Avda. Gral. Paz 1499, 1650 San Martín, Pcia. Buenos Aires, Argentina

^c CONICET, Avda. Rivadavia 1917, 1033 Buenos Aires, Argentina

^d UNSAM/CNEA, Intituto Sabato, Avda. Gral. Paz 1499, 1650 San Martín, Pcia. Buenos Aires, Argentina

^e Saint-Petersburg State Polytechnical University, Experimental Nuclear Physics Department, K-89, Faculty of Physics and Mechanics, 29 Polytekhnicheskaya Str., 195251, St. Petersburg, Russia

^f Université Libre de Bruxelles, Physique des Solides Irradiés et des Nanostructures CP234, Faculté des Sciences, Bd du Triomphe, B-1050 Bruxelles, Belgium

ARTICLE INFO

Article history:

Received 1 January 2011

Received in revised form 16 February 2011

Accepted 21 February 2011

Available online 22 March 2011

Keywords:

Phase diagram

Miscibility gap

Spinodal gap

Thermodynamic integration

Atomistic methods

Iron chromium

ABSTRACT

Prior to applying any interatomic potential, it is important to know the stability of the different phases it describes. In the literature many methods to determine the phase diagram from an interatomic potential are described. Although for pure elements the procedure to obtain the thermodynamic functions is well established, for alloys it is not. In this work a method is developed to determine the phase diagram, i.e., solubility limits and spinodal gap, for the case of miscibility gaps. The method combines Monte Carlo simulations in the isobaric semi-grand canonical ensemble, full thermodynamic integration and Redlich–Kister expansions to parameterize the Gibbs free energy. Besides numerical inaccuracies, this method does not rely on any physical approximations to determine the phase diagram of a given interatomic potential. The method is applied to two different Fe–Cr potentials that are widely used in the literature. The resulting phase diagrams are discussed by comparing them to the experimental one and ones obtained in other works from the same potentials.

© 2011 Elsevier B.V. All rights reserved.

1. Introduction

Prior to applying any interatomic potential, it is important to know the stability of the different phases it describes. In the literature many methods to determine the phase diagram from interatomic potentials are described. For pure elements the procedure to obtain the thermodynamic functions is well established; for example using the coupling parameter method based on either molecular dynamics (MD) or Monte Carlo (MC) simulations [1–4]. For (binary) alloys, however, the situation is less clear.

In the literature there are some examples where the authors have extended the thermodynamic integration procedure to alloys, with mixed success [5–7]. The major drawback of such procedures is the decoupling between vibrational and configurational entropy as both are calculated independently from each other. In addition, the configurational entropy is approximated by the ideal solution or a cluster variation method expression [8]. Other procedures rely on MC simulations in the canonical ensemble (N, V, T) to estimate the phase boundaries from the identification of phase

separation [9,10] or the determination of the thermodynamic functions [11]. The main shortcoming of the latter procedures is their need to operate in coexisting phase conditions. Due to the finite size of a simulation box, the obtained thermodynamic functions are susceptible to interface effects and are therefore inherently box size dependent.

The most appropriate method when dealing with solid solutions are MC simulations in the isobaric semi-grand canonical ensemble ($N, P, T, \Delta\mu$). This method does not suffer from interface effects since the fixed chemical potential difference guarantees single phase regime. The aim is to obtain (at a given temperature) the equilibrium concentration of a given phase as a function of the chemical potential difference. Any discontinuity observed in such a curve is then associated with a phase transition, with the concentration just before and after the transition indicating the solubility limits [12]. Such procedures work well when the transformation barrier for nucleation of the new phase is low. In the other cases, however, the solubility limits cannot be determined unambiguously since hysteresis occurs, i.e., the location of the discontinuity depends essentially on the initial phase from which the simulation was started. Also, in the particular case of miscibility gaps, it is impossible to estimate the spinodal gap from the latter procedure.

* Corresponding author. Tel.: +32 14 333197; fax: +32 14 321216.

E-mail address: gbonny@sckcen.be (G. Bonny).

To overcome these problems, in this work a methodology to determine the solubility limits and spinodal gap in the case of miscibility gaps is established. We combine MC simulations in the isobaric semi-grand canonical ensemble, full thermodynamic integration techniques and the theory of Redlich–Kister expansions to determine the Gibbs free energy curves, from which the phase diagram is determined. Besides numerical inaccuracies, the applied procedure does not rely on any physical approximations.

The method is illustrated on two different interatomic potentials fitted to the iron–chromium system. This system exhibits a miscibility gap (with high transformation barrier for nucleation of the second phase [13]), which has recently received renewed interest as high-Cr steels are candidate structural materials for nuclear applications [14]. The (Fe, Cr) alloy exhibits a large Cr solubility ($\sim 9\%$ Cr) [15], which is in the composition range of technological applications (5–12%Cr) [14]. From the modelling viewpoint, it is therefore important to establish as precisely as possible the phase diagram associated with the different Fe–Cr potentials.

The paper is organised as follows; in Section 2 a brief overview of the used methods is given. In Section 3 the followed procedure to obtain the thermodynamic functions and corresponding phase diagram given an interatomic potential is explained. In Section 4 the results of the former procedure on the different Fe–Cr potentials are presented and the obtained phase diagrams are compared to the Calphad calculated one. In Section 5 the phase diagrams obtained in the present work are compared with the ones from previous works. Based on this comparison the performance of the present method is discussed.

2. Methodology

2.1. Cohesive model

The atomic interactions of the iron–chromium system are described using the two-band model (2BM) [16]. This model is known to be capable of describing an alloy's complex behaviour – such as the (Fe, Cr) system – with composition [17], for example mixing enthalpy, short-range order parameter, etc. The 2BM constitutes of the standard embedded atom method (EAM) extended with an extra embedding term that accounts for contributions from the *s*-band electronic density to the cohesive energy.

In this work two such type of potentials that are available in the literature are used, namely, the one fitted by Olsson et al. [16,18] (henceforth OLS) and its recent refit by Bonny et al. [19,20] (henceforth BON). In both cases the potentials were fitted accounting for (amongst many other properties) thermodynamics and should therefore give a reasonable description of the thermodynamic functions as obtained from both experiments and density functional theory (DFT) data.

The pure elements (Fe and Cr) are described by the EAM potentials fitted by Ackland et al. [21] (Fe part of OLS), Mendeleev et al. [22] (Fe part of BON), Olsson et al. [16] (Cr part of OLS) and Bonny et al. [19,20] (Cr part of BON). They all constitute the present state-of-the-art EAM potentials for Fe and Cr (see [23] for a review on the Fe parts).

2.2. Isobaric Monte Carlo in semi-grand canonical ensemble

Metropolis Monte Carlo (MC) sampling [24] within the isobaric semi-grand canonical ensemble ($N, P, T, \Delta\mu$) is used to estimate the equilibrium concentration of a given phase containing N atoms at a given temperature T , pressure P and chemical potential difference $\Delta\mu$. The MC method includes three types of trials: (i) a random displacement of all atoms from their current positions (by this trial lattice relaxation and vibrational entropy are accounted for); (ii)

the change of species of a randomly picked atom (by this trial the equilibrium composition is sampled); (iii) the overall volume change of the simulation box (this trial allows the desired pressure to be maintained, even if a structural transition were to occur). The decision on the acceptance of the new configuration is based on the standard Metropolis algorithm [24] and one set of these trials is termed an “MC step”.

All MC simulations were performed starting from bcc crystals containing $N = 1024$ atoms, at $P = 0$ Pa, in the ranges $T = 300$ – 1200 K, $\Delta\mu = \mu_{\text{Cr}} - \mu_{\text{Fe}} = -0.25$ – -0.35 eV and under periodic boundary conditions along the three principal directions. They were performed until convergence in concentration and its variance was reached, which typically takes $\sim 2 \times 10^5$ – 2×10^6 MC steps.

2.3. Thermodynamic integration

The Gibbs free energy $G(T)$ (henceforth free energy) of the pure elements is calculated using a coupling parameter method which relates the free energy of a desired state to a reference state along a (quasi-) adiabatic path. As the reference state the Einstein crystal at 300 K is chosen for which the free energy can be determined exactly [1]. The appropriate spring strengths associated with the Einstein oscillators for the Fe and Cr potentials were determined from MD runs in canonical ensemble (N, V, T), as explained in [25]. After equilibration of such a reference state with free energy $G_{\text{Einstein}}(300 \text{ K})$, dynamic adiabatic switching [3] was used to switch quasi-statically between the reference and the real system as to obtain its free energy, $G_{\text{Real}}(300 \text{ K})$.

Secondly, $G_{\text{Real}}(300 \text{ K})$ is used as reference state to apply reversible scaling [4] between the latter and the real system as to obtain its free energy at 1500 K, $G_{\text{Real}}(1500 \text{ K})$. Using this procedure, the free energy of the real system $G_{\text{Real}}(T)$ is obtained as a function of temperature in the interval 300–1500 K.

Both switching procedures were applied on bcc simulation crystals containing 2000 atoms. Typical equilibration times of initial and final states – $G_{\text{Einstein}}(300 \text{ K})$, $G_{\text{Real}}(300 \text{ K})$ and $G_{\text{Real}}(1500 \text{ K})$ – were ~ 10 ps and the typical switching time between two states was 25 ps and 150 ps for the first and second switching procedure, respectively. For both switching procedures the forward and backward path was calculated. The enclosed surface between both curves represents the irreversible work performed due to the finite switching time and is a measure for the precision of the obtained free energy. From these cycles it was checked that for the above parameters the error on the free energy is of the order 1 meV/atom.

3. Phase diagram calculation

Firstly, the aim is to obtain the equilibrium concentration of the different phases (in our case the α and α' phases) as a function of chemical potential difference $\Delta\mu = \mu_{\text{Cr}} - \mu_{\text{Fe}}$ in the temperature range of interest (until full solubility is observed). This is done by performing MC simulations in the isobaric semi-grand canonical ensemble, as described in Section 2.2. At temperatures within the miscibility gap, such a curve typically exhibits a discontinuity that indicates a phase transition. The value of $\Delta\mu$ for which this transition occurs can depend (for high transformation barriers for nucleation of the new phase) on the initial phase from which the simulations were started, i.e., pure Fe or Cr. This effect is known as hysteresis and is visualised by repeating the procedure twice, once starting from pure Fe and Cr, respectively. Particularly at low temperature this effect is non-negligible (see for example Fig. 1a). The temperature for which full solubility is observed is identified by continuity and the lack of hysteresis of the equilibrium concentration with $\Delta\mu$. Clearly this indicates single phase regime (see for example Fig. 1b).

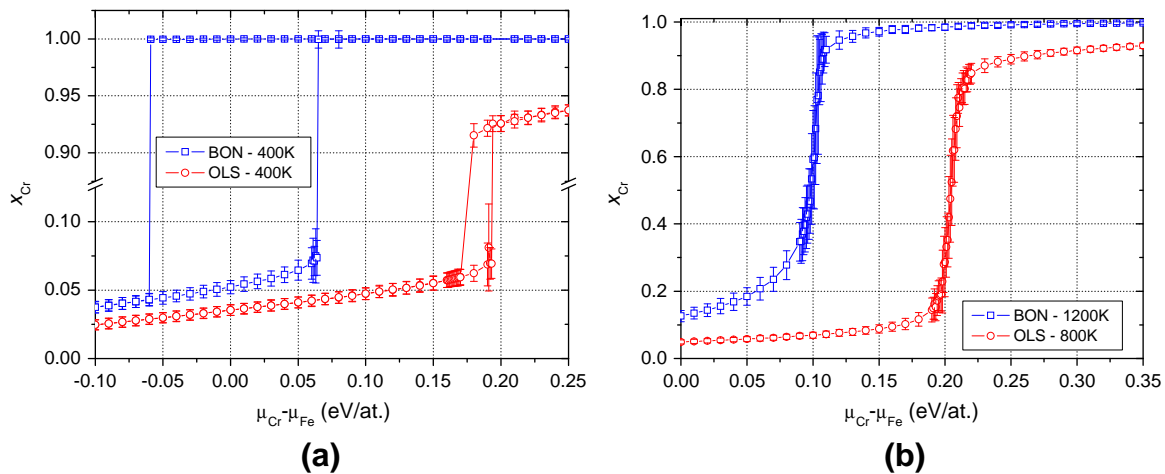


Fig. 1. Composition of the α and α' phases as a function of chemical potential difference for both potentials; (a) within the miscibility gap and (b) above it.

The chemical potential difference $\Delta\mu$ in turn is the first derivative of the Gibbs free energy $G(x)$ with respect to concentration, x ($x = x_{\text{Cr}}$),

$$\Delta\mu(x) = \frac{\partial G(x)}{\partial x}. \quad (1)$$

By integration of Eq. (1), $G(x)$ is obtained up to an additive constant. Practically, $G(x)$ is represented following the Calphad methodology [26] as:

$$G(x) = x_{\text{Cr}}G_{\text{Cr}}(T) + x_{\text{Fe}}G_{\text{Fe}}(T) + k_{\text{B}}T(x_{\text{Cr}} \ln x_{\text{Cr}} + x_{\text{Fe}} \ln x_{\text{Fe}}) + x_{\text{Fe}}x_{\text{Cr}} \sum_{p=0}^M L_p(x_{\text{Cr}} - x_{\text{Fe}})^p. \quad (2)$$

Here the first two terms represent the free energy of the mechanical mixture with G_{Fe} (G_{Cr}) the Gibbs free energy for pure Fe (Cr); the third term is the configurational entropy for an ideal solution with k_{B} Boltzmann's constant; and the fourth term is a Redlich–Kister (RK) expansion [27] accounting for deviations from the ideal solution, with L_p RK coefficients and M the order of the RK expansion. As shown in [26,28], such an expansion is suitable to describe disordered and short-range ordered solid solutions.

Secondly, the Gibbs free energy of the pure phases – first and second terms in Eq. (2) – is determined using the full thermodynamic integration described in Section 2.3 (see for example Fig. 2). Given the latter, the derivative of Eq. (2) is fitted to the

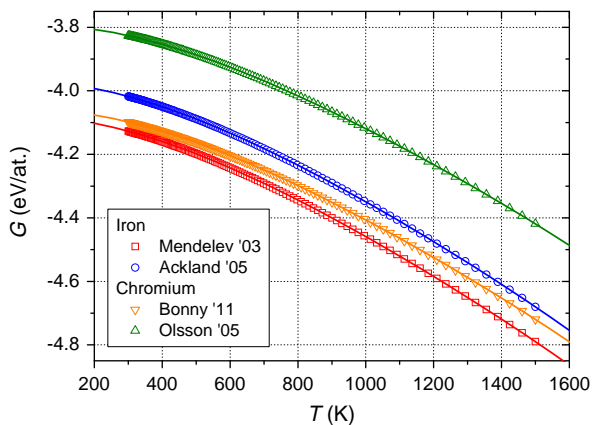


Fig. 2. Free energy calculated by a full thermodynamic integration (see Section 2.3) for all four potentials describing the pure elements.

resulting curves for the α and α' phases at each calculated temperature, where the RK coefficients are the only remaining fitting parameters. From the resulting free energy curves, the solubility limits are determined by a common tangent construction.

To ensure the high precision on $G(x)$ needed to determine the solubility limits, a different RK expansion was fitted for the α and α' phase (see for example Fig. 3a). Here M typically takes values between 3 and 5. It should be noted that each curve was visually inspected to guarantee that no unphysical oscillations occur in the concentration range of interest.

To obtain an estimate for the spinodal gap, $G(x)$ must be fitted by a single RK expansion for both the α and α' phases, as the spinodal gap is determined from the flexing points of $G(x)$ (see for example Fig. 3b). To avoid unphysical oscillations M was limited to three, which provides reasonable fits at low temperature (<500 K) but lacks precision above. Due to this limitation the location of the spinodal gap is only indicative. It should also be noted that, although presently used in the fit, G_{Fe} and G_{Cr} are not strictly necessary when a single RK expansion is fitted to describe both α and α' phases.

4. Results

In Fig. 1 typical plots of x_{Cr} versus $\Delta\mu$ are shown for BON and OLS. Similar figures (not all shown) were plotted in steps of 100 K for temperatures from 300 K up to 800 K and 1200 K – where full solubility is observed – for OLS and BON, respectively. In all figures, the error bars are taken as the 95% confidence interval for the average concentration obtained from the MC simulations (i.e., twice the standard deviation around the mean value). The resolution on the $\Delta\mu$ axis was 10 meV and 1 meV in the vicinity of a possible phase transition.

In Fig. 1a typical curves for temperatures inside the miscibility gap are shown (400 K). For both potentials a clear discontinuity – indicating a phase transition – well outside the error bars is observed. From the figure it is clear that (particularly for BON) the hysteresis effect mentioned in Section 3 does not allow an unambiguous determination of the solubility limit. In Fig. 1b typical curves for temperatures above the miscibility gap are shown (800 K for OLS and 1200 K for BON). In these cases no hysteresis is observed and each curve describes the whole concentration range continuously, which indicates full solubility.

In Fig. 2 the free energy calculated from the full thermodynamic integration (see Section 2.3) is plotted for all four potentials describing the pure elements. Each curve consists of two data sets

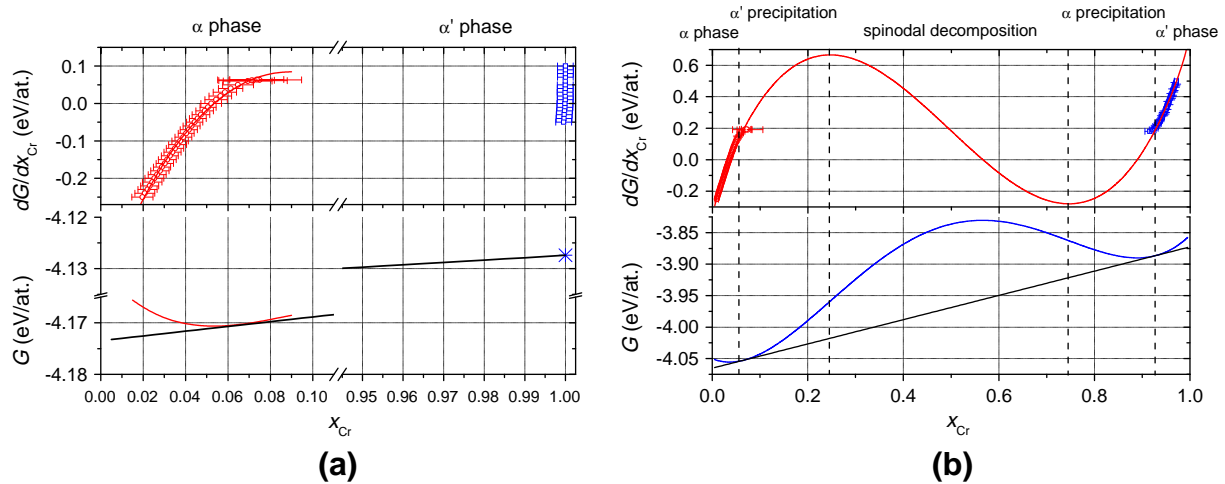


Fig. 3. Illustration of the free energy (lower panel) and its derivative (top panel) at 400 K using BON (a) and OLS (b).

representing the full switching cycle. Although both data sets are plotted, they cannot be distinguished as they do not differ by more than 1 meV. The full curves are polynomial interpolations of both data sets. For practical reasons it is these curves that enter the RK expansion (G_{Fe} and G_{Cr}), but it is emphasized that these interpolations do not affect the overall precision.

In Fig. 3 the free energy (lower panels) and its derivative (top panels) is illustrated for BON (a) and OLS (b) at 400 K. In the top panels the quality of the RK fit to $\Delta\mu$ is illustrated, i.e., the RK fits are well within the error bars. In Fig. 3a one RK expansion per phase was fitted to ensure a high quality fit to determine the phase boundaries while in Fig. 3b a single RK expansion was fitted to both phases as to determine the spinodal gap. At the present temperature, for both cases the RK expansions fall well within the MC obtained error bars. For high temperatures (>500 K) this is only true if one RK expansion is fitted per phase. In the lower panels the resulting Gibbs free energy is plotted together with the common tangent construction indicating the solubility limits of the miscibility gap. In Fig. 3b, besides the latter, the spinodal region is also indicated.

The phase diagrams – miscibility gap and spinodal gap – calculated from both potentials are compared to a recently proposed parameterization based on the Calphad methodology [6] in Fig. 4. The Calphad miscibility gap is calculated from an experimentally based [15,29] Gibbs free energy parameterization. The error bars were taken from the corresponding $\Delta\mu$ versus x_{Cr} curves (see for

example Fig. 3) at the compositions obtained from the common tangent constructions.

When focused on the Calphad curve in the Fe-rich region, large Cr solubility at low temperature is observed. As shown in Fig. 4, this behaviour is well reproduced by both potentials. At about 750 K the Fe-rich solubility limit of the Calphad curve increases until full solubility is observed above the critical temperature ~ 900 K. The curve resulting from OLS underestimates this critical temperature by ~ 200 K while BON overestimates it by roughly the same amount. The difference in critical temperature between OLS and BON is mainly attributed to their difference in the excess vibrational entropy, as discussed in [19].

On the Cr-rich side, the Fe solubility following from the Calphad curve approaches zero with decreasing temperature, which is reproduced by BON but not by OLS. The latter predicts high Fe solubility as an unphysical artefact of a negative heat of mixing at the Cr-rich side (see [19,25] for an extended discussion).

Regarding the spinodal gap, all models (potentials and Calphad) follow the shape of the miscibility gap but shifted towards the centre by $\sim 20\%$. It is only at ~ 100 K below the transition temperature towards full solubility that the miscibility gap converges to the spinodal one. Since the same behaviour is observed for the Calphad model and the potentials, our method to estimate the spinodal gap seems reasonable. However, we emphasize that the spinodal gaps are only indicative as they rely on the extrapolation capabilities of

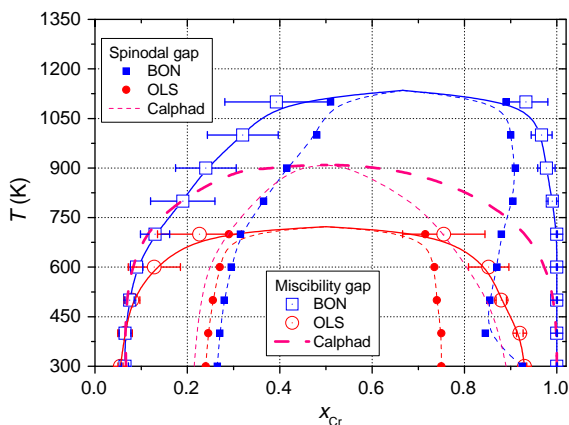


Fig. 4. Comparison of the phase diagrams resulting from the potentials with the latest Calphad parameterization.

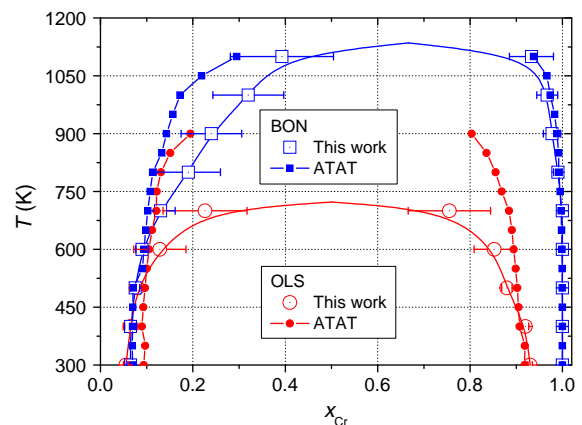


Fig. 5. Comparison of the miscibility gap obtained in this work with previous ATAT calculations.

the RK expansion and the Calphad parameterization was not fitted to it.

5. Discussion and concluding remarks

In a previous work [25] the phase diagram resulting from OLS was already calculated using indirect but computationally inexpensive methods. For the sake of comparison, the same methods were also applied to BON. Briefly, the phase diagram was estimated using the (freely available) ATAT package [30,31], which was interfaced to an in-house MD code working as 'energy engine'. The package works in two stages: firstly, an automated statistically optimised procedure is followed in order to build a cluster expansion of the configuration energy on the bcc lattice (this is where the MD code, namely the interatomic potential, enters); secondly, the previous expansion is fed to a rigid lattice MC code working in semi-grand canonical ensemble for tracking the phase boundaries. The cluster expansion is here used as an economical way to compute the configuration energy of any configuration of the simulation box. The method implicitly accounts for the configurational entropy but neglects vibrational entropy. To account for this shortcoming, vibrational entropy calculated from separate MD runs [25] or a harmonic analysis [32] on random alloys was indirectly included by making the cluster expansion temperature dependent [25]. In this way vibrational entropy is effectively included, although it is decoupled from the configurational entropy.

The phase diagrams from the latter procedure are compared with the ones presented here in Fig. 5. Given the error bars, the ATAT curves follow the ones of the present work well below 700 K for OLS and up to full solubility for BON. For OLS, the critical temperature for full solubility resulting from ATAT is overestimated by ~ 200 K compared to the one presented here. Judging from the difference between both procedures to estimate the phase diagram, it seems that vibrational and configurational entropy are coupled stronger for OLS than for BON.

In a previous work harmonic analysis of random alloys has shown that the excess vibrational entropy from OLS is about twice larger than that from BON [19]. Thereby the former amounts to about half the configurational entropy. These results in combination with our observation from Fig. 5 suggest that the coupling strength between excess vibrational and configurational entropy strongly depends on the ratio between both, with strongest coupling when their ratio approaches one.

To conclude, the following recommendations seem in place: (i) when excess vibrational and configurational entropy are strongly coupled, i.e., of similar size (for simplicity) evaluated on random solutions, then the methodology developed in the present work should be followed; (ii) when the former are weakly coupled, i.e., essentially different in size, then the ATAT method probably provides a reasonable estimate. It should be noted that the high accuracy of the presented method comes at the cost of an increase of the computational load by about an order of magnitude compared to the ATAT method.

Acknowledgements

This research has received partial funding from the European Atomic Energy Community's 7th Framework Programme (FP7/2007-2011), under grant agreement number 212175 (GetMat project). It also contributes to the European Fusion Technology programme (EFDA). The work was partially sponsored by the Belgo-Argentine FWO-MINCYT bilateral cooperation agreement, Project VS.004.10N. The calculations were partially performed on the HPC cluster Jülich within the APM project. EEZ acknowledges support from the Consortium of the Erasmus Mundus Master FUSION-EP.

References

- [1] D. Frenkel, B. Smit, *Understanding Molecular Simulations—From Algorithms to Applications*, Academic, London, 1996.
- [2] D. Frenkel, A.J.C. Ladd, *Journal of Chemical Physics* 81 (1984) 3188.
- [3] M. deKoning, A. Antonelli, *Physical Review E* 53 (1996) 465.
- [4] M. de Koning, A. Antonelli, S. Yip, *Journal of Chemical Physics* 115 (2001) 11025.
- [5] E. Arregui, M. Caro, A. Caro, *Physical Review B* 66 (2002).
- [6] G. Bonny, P. Erhart, A. Caro, R.C. Pasianot, L. Malerba, M. Caro, *Modelling and Simulation in Materials Science and Engineering* 17 (2009).
- [7] E. Lopasso, M. Caro, A. Caro, P. Turchi, *Physical Review B* 68 (2003).
- [8] K. Kikuchi, *Physical Review* 81 (1951).
- [9] E.E. Zhurkin, R. Pereira, N. Castin, L. Malerba, M. Hou, *Materials for Future Fusion and Fission Technologies* 1125 (2009) 121.
- [10] L. Malerba et al., *Journal of ASTM International* 4 (2007).
- [11] F.M. Marquez, C. Cienfuegos, B.K. Pongsaï, M.Y. Lavrentiev, N.L. Allan, J.A. Purton, G.D. Barrera, *Modelling and Simulation in Materials Science and Engineering* 11 (2003) 115.
- [12] S.M. Foiles, M.S. Daw, *Journal of Materials Research* 2 (1987) 5.
- [13] G. Bonny, D. Terentyev, L. Malerba, D. Van Neck, *Physical Review B* 79 (2009).
- [14] A. Kohyama, A. Hishinuma, D.S. Gelles, R.L. Klueh, W. Dietz, K. Ehrlich, *Journal of Nuclear Materials* 237 (1996) 138.
- [15] G. Bonny, D. Terentyev, L. Malerba, *Scripta Materialia* 59 (2008) 1193.
- [16] P. Olsson, J. Wallenius, C. Domain, K. Nordlund, L. Malerba, *Physical Review B* 72 (2005) 214119.
- [17] G. Bonny, R.C. Pasianot, L. Malerba, *Philosophical Magazine* 89 (2009) 711.
- [18] P. Olsson, J. Wallenius, C. Domain, K. Nordlund, L. Malerba, *Physical Review B* 74 (2006) 1 (E).
- [19] G. Bonny, R.C. Pasianot, D. Terentyev, L. Malerba, *Philosophical Magazine*, in press, doi:10.1080/14786435.2010.545780.
- [20] D. Terentyev, G. Bonny, C. Domain, R.C. Pasianot, *Physical Review B* 81 (2010).
- [21] G. Ackland, M. Mendeleev, D. Srolovitz, S. Han, A. Barashev, *Journal of Physics: Condensed Matter* 16 (2004) 1.
- [22] M. Mendeleev, S. Han, D. Srolovitz, *Philosophical Magazine* 83 (2003) 3977.
- [23] L. Malerba et al., *Journal of Nuclear Materials* 406 (2010) 19.
- [24] M.P. Allen, D. Tildesley, *Computer Simulation of Liquids*, Clarendon Press, Oxford, 1987.
- [25] G. Bonny, R.C. Pasianot, L. Malerba, A. Caro, P. Olsson, M.Yu. Lavrentiev, *Journal of Nuclear Materials* (2009).
- [26] N. Saunders, A.P. Miodownik, *CALPHAD Calculation of Phase Diagrams: A Comprehensive Guide*, Pergamon, Kidlington, 1998.
- [27] O. Redlich, A.T. Kister, *Industrial and Engineering Chemistry* 40 (1948) 345.
- [28] G. Bonny, D. Terentyev, L. Malerba, *Journal of Phase Equilibria and Diffusion* 31 (2010) 439.
- [29] J. Andersson, B. Sundman, *Calphad* 11 (1987) 83.
- [30] A. van de Walle, M. Asta, *Modelling and Simulation in Materials Science and Engineering* 10 (2002) 521.
- [31] A. van de Walle, G. Ceder, *Journal of Phase Equilibria* 23 (2002) 348.
- [32] A. van de Walle, G. Ceder, *Reviews of Modern Physics* 74 (2002) 11.